USE OF OBLIQUELY ROTATED PRINCIPAL COMPONENT ANALYSIS TO IDENTIFY COHERENT STRUCTURES

DONALD K. RINKER, JR. and GEORGE S. YOUNG
Department of Meteorology, The Pennsylvania State University, University Park, PA, U.S.A.

(Received in final form 19 February, 1996)

Abstract. Principal component analysis (PCA) with oblique rotation is applied to Large Eddy Simulation (LES) results to discern and quantify coherent structures within the convective boundary layer (CBL). Sensitivity tests are first conducted on a moderately convective LES run. Once the ability of PCA to generate robust results is verified, the method is applied to LES runs spanning a range of stability regimes. Interregime similarities and differences in the coherent structures are discussed. For the moderately convective LES run, three-dimensional convective cells are arrayed in two-dimensional bands aligned with the geostrophic wind. The resulting gravity waves in the free atmosphere and convective inflow and outflow in the boundary layer are also captured by the PCA. Convective modes are more sensitive to the ratio of w_* to u_* than are the dynamic modes.

PCA has demonstrated advantages over previous analysis methods. PCA score maps provide information on the spatial distribution of phenomena that has not been available from traditional conditional sampling studies. Principal components provide information on the vertical structures of phenomena that would be obscured by life-cycle effects or erratic tilts from the vertical in the conventional approaches to either conditional sampling or composite analysis. Future work includes application of this technique to multi-level observational time series from a surface-layer tower for the Risø Air/Sea Experiment (RASEX).

1. Introduction

Quantitative descriptions of coherent structures in the turbulence field are fundamental to our understanding of the atmospheric boundary layer, as these phenomena are responsible for the majority of the vertical fluxes at all levels in the boundary layer (Young, 1988; Khalsa and Greenhut, 1985). In the mixed layer, the dominant structures, boundary-layer spanning convective cells and rolls, are composed of buoyantly driven updrafts and downdrafts (Young, 1988). The related convective elements within the surface layer, called ramps or plumes, have horizontal and vertical scales on the order of the surface-layer depth (Weijers *et al.*, 1995). In the capping inversion and stable free atmosphere, gravity waves dominate the coherent structure population. Because these dynamically distinct phenomena can coexist in time and space, separating them for quantitative analysis is a critical problem.

In attempting to solve this problem, investigators have employed many methods of data acquisition. Observational techniques include the use of laboratory tanks and wind tunnels (Deardorff and Yoon, 1984) and field experiments using towers, aircraft, and tethered balloons (Kaimal *et al.*, 1976; Wilczak, 1984; Khalsa and Greenhut, 1985). Large eddy simulation (LES) has also been used to acquire data for the study of coherent structures (Deardorff, 1972; Schmidt and Schumann, 1990; Moeng and Schumann, 1991; Schumann and Moeng, 1991a). By definition,

Boundary-Layer Meteorology **80:** 19–47, 1996.

these models have resolutions sufficiently finer than the size of the largest eddies to ensure accurate representations of the coherent structures. LES data are used in the analysis in this paper because they alone provide the three-dimensional multivariate data required for assessments of the utility of the method and full interpretation of the results. Once the utility of the method is verified, it will be applicable to data from towers, tethered balloons, and remote sensors.

2. Procedures

The data sets used in this research are taken from LES output. A LES code explicitly calculates the large-eddy field and parameterizes the small (subgrid) eddies. The LES approach has been popular for the study of the atmospheric boundary layer because the large eddies represented therein are generally responsible for most of the turbulent transport and other aspects of turbulent dynamics (Moeng, 1984; Young, 1988; Sikora and Young, 1993). The LES results are therefore believed to be relatively insensitive to the parameterization scheme for small eddies (Moeng, 1984), at least for levels above the surface layer. Because LES resolution is significantly finer than the size of the largest, and thus, most coherent eddies, the LES approach ensures accurate representations of at least those coherent structures occurring on the scale of the boundary-layer depth. LES has, therefore, been used successfully to acquire data for the study of coherent structures in the boundary layer (Moeng and Schumann, 1991; Schumann and Moeng, 1991a).

The LES code used in this study is derived from that of Moeng (1984) and is used because this LES version has demonstrated an ability to describe coherent structures accurately (Moeng and Schumann, 1991; Schumann and Moeng, 1991a). Moeng's model uses Fourier expansions in the horizontal directions and finite differencing in the vertical. The subgrid fluxes are related to the resolvable fields using subgrid-scale eddy coefficients. The upper boundary conditions are $w = 0$, $\partial u/\partial z = 0$, $\partial v/\partial z = 0$, $\partial \theta/\partial z =$ constant, and zero subgrid-scale turbulence fields. The domain size is 3 km by 3 km in the horizontal and 1 km in vertical. Boundary-layer depth, Z_i, for the runs studied is 500 m. The domain is therefore 6 Z_i in the horizontal and $2Z_i$ in the vertical.

Specification of the scaling parameters for shear and buoyant production of turbulent kinetic energy (TKE) allows each LES run to reflect a dynamically different turbulence regime. Thus, these data provide the basis for discerning the regime dependence of convective boundary-layer coherent structures.

Because different scaling parameters are used in each run of the LES, the turbulent structure for each data set is representative of a distinct environment. Three distinct environments are examined in this research. As can be seen from Table I, there is a strongly convective case (case 4), a moderately convective case (case 2a), and a slightly weaker convective case (case 5). Although convective, all of these cases have significant shear production as measured by u_*, i.e., there is

Table I

Comparison of the scaling parameters for the different convective regimes. u_* is the friction velocity in ms^{-1}, $w'\theta'_0$ is the surface temperature flux in K ms^{-1}, and w_* is the convective velocity scale in ms^{-1}

Case	u_* (ms^{-1})	$w'\theta'_0$ (K ms^{-1})	w_* (ms^{-1})
2a	0.5584	0.05	0.9415
4	0.5609	0.24	2.0144
5	0.5747	0.03	0.7775

enough shear production for it to be an important element in convective boundary layer dynamics based on the ratio of u_* to w_*. Comparison of the results from these three cases provides the basis for determining if related families of coherent structures appear in all three regimes. This analysis tests the hypothesis that there are certain structures inherent to convection, be the buoyant production weak, moderate, or strong relative to the shear production. In examining the results from these three cases, emphasis is placed on determining the impact of the ratio of buoyant production to shear production on the form and dynamics of the coherent structures.

To test the robustness of the results, another LES data set was acquired from the same LES run as case 2a; it is, however, separated in time by about one large-eddy turnover time from that used in case 2a. This data set is designated as case 2b. It was acquired to see how sensitive the results for a particular environment are to the details of a particular turbulence realization.

Once the data sets are obtained, the question becomes how to analyze the properties of coherent structures in the simulated boundary layers. This task has been traditionally accomplished through conditional sampling and/or composite analysis (Wilczak and Tillman, 1980; Lenschow and Stephens, 1980; Khalsa, 1980; Greenhut and Khalsa, 1982; Wilczak, 1984; Khalsa and Greenhut, 1985; Khalsa and Greenhut, 1987; Greenhut and Khalsa, 1987; Young, 1988; Schumann and Moeng, 1991a; Schumann and Moeng, 1991b; Sikora and Young, 1993). However, as Weijers *et al.* (1995) and Moeng and Schumann (1991) point out, different methods of conditional sampling and composite analysis often lead to different results. Thus, a more objective technique is needed.

This research addresses the objectivity question by applying principal component analysis (PCA) (Richman, 1986) to the LES data sets. By using PCA, the categories of coherent structures found depend on the data themselves rather than on the authors' preconception of what phenomena to sample. Put simply, the application of PCA used here decomposes the multivariate profiles that make up the original data into a horizontally-dependent linear combination of empirical orthogonal basis vectors which are called principal components (PCs). These basis vectors are the eigenvectors of a covariance matrix computed from a data matrix contain-

ing multivariate profiles from a single time step in LES results. Some investigators use a correlation matrix (which is created in the same manner as the covariance matrix, but is formed using normalized values for each variable); however, use of a covariance matrix reduces sensitivity to noise in the data (Richman, 1986), so that method is applied here. From this covariance matrix, eigenvalues and the corresponding eigenvectors are found. As stated above, the eigenvectors of the covariance matrix are the unrotated PCs. Thus, these unrotated PCs are basis functions of the original data set of the multivariate profiles through the LES domain; then linear combinations of the unrotated PCs can be used to describe and reconstruct these data profiles. The coefficients used in this reconstruction are called PC scores. For this analysis, the scores form maps in the horizontal domain (x, y) of the relative importance of the corresponding PCs. This data reconstruction can also be accomplished after applying either an orthogonal or oblique rotation to the PCs.

While any analysis is to some extent subjective because of the need for physical understanding by the analyst, PCA requires physical understanding only for the final stage, subjective interpretation of results. In contrast, most prior methods also require a healthy dose of physical understanding for the design and tuning of the data analysis method itself. Thus, the use of PCA ensures that the analyst's biases do not affect the quantitative results, only their subjective physical interpretation. Despite the relative objectivity of PCA, options do exist for the subsequent rotation of the principal components. Unrotated PCA is useful merely as a dimension reduction technique, and is ineffectual for identifying modes of variability of physical data (Jolliffe, 1987). Burroughs and Miller (1961) and Cattell and Dickman (1962) state that if the objective of PCA is to capture the physics behind the data set, then it is necessary to rotate the principal component vectors until each of these vectors points at (i.e., highly correlated with) a distinct cluster of observations, thereby achieving what is commonly called simple structure. This rotation takes place in the vector space spanned by the original data vectors. The complete set of PC vectors also spans this vector space. Before rotation and after orthogonal rotation the PCs also form a mutually perpendicular set of axes within this vector space. Each cluster of observations towards which a PC is rotated is a group of data vectors pointing in the same general direction within this vector space. The data vectors in such a cluster do not need to be of similar lengths. Thus, each point in a cluster represents a data profile that is similar in form, if not in amplitude, to the other data profiles in its cluster. These points need not be adjacent in physical space (i.e. within the LES domain). For the multi-PC phenomena described later in this section, the corresponding cluster of data points spreads across a vector subspace with as many dimensions as there are PCs needed to describe the phenomena.

The choice of rotation for this study stems from a study by Richman (1986), who tested various commonly used rotation schemes for their ability to uncover coherent structures in meteorological fields. An oblique rotation named Promax, which achieves a simple structure solution, proved to be one of the two most

accurate in comprehensive tests by Richman (1986). Based on this result, the Promax rotation was chosen for this research.

An option also exists for determining the number of principal components to rotate. The literature describes many ways to decide on this number. This research uses the scree test (Cattell, 1958) as it is generally thought to be an optimal choice for distinguishing those PCs that are dominated by meaningful signal from those dominated by noise. Such a separation of the PCs is required in most geophysical situations. The only PCs that should be retained for rotation are those that contribute significantly to the signal variance and are not dominated by noise. The scree test detects the desired PCs based on the distinct characteristics of signal PCs and noise PCs on an eigenvalue plot. In the scree test, the eigenvalues associated with the PCs are plotted in order of decreasing magnitude. Such a graph is generally composed of two quasi-linear segments; the one at large eigenvalues with a steeper slope and the one at small eigenvalues with a more gradual slope. The region of gradual slopes arises from the tendency for noise to distribute itself uniformly across PCs. Thus, the gradual slope in a section of the eigenvalue plot implies noise domination of the corresponding PCs, while a steeper slope implies signal domination of the corresponding PCs. The PCs retained are, therefore, those in the steep-slope portion of the graph, including the PC where the steeper slope joins the gradual slope. An example of a scree test eigenvalue plot is given in Figure 1. In cases in which it is not precisely clear from breaks in the figure's slope how many factors to rotate, it is best to rotate as many factors as the most liberal interpretation of the scree test allows (Dingman *et al.* 1964). This overfactoring does not significantly affect solutions of oblique rotations (Dingman *et al.*, 1964).

PCA is known to work best on problems where the phase (location) of the coherent structures is constrained relative to the bounds of the analysis domain (Richman, 1986). Thus, the analysis technique is applied to vertical profiles rather than horizontal fields so as to take advantage of the boundedness imposed by the surface and capping inversion. The LES data are arranged in a $96\times96\times96$ grid so 96×96 such profiles are available at each time step. Because the model grid spacing is much less than the integral length scale, adjacent profiles are highly correlated. Therefore, little information is lost by analyzing only every fourth profile (in the x- and y-directions), yielding 576 semi-independent cases. Each profile contains 72 levels extending from the surface to $1.5Z_i$, where Z_i is depth of the boundary layer, and $1.5Z_i$ is three-quarters of the domain depth. Thus, both the mixed layer and the inversion layer are included in the profiles, thereby allowing the analysis of both convection and gravity waves. The layers near the upper boundary of the domain are avoided, however, as the impact of the upper boundary conditions on the coherent structures is uncertain. The profiles include perturbation values of horizontal velocity, vertical velocity, and temperature, yielding a 576 by 288 data matrix. This matrix provides a multivariate snapshot of the large-eddy field.

Unfortunately, the resulting matrix is so large that computer memory limits are exceeded. This problem is corrected by taking every other level in the vertical

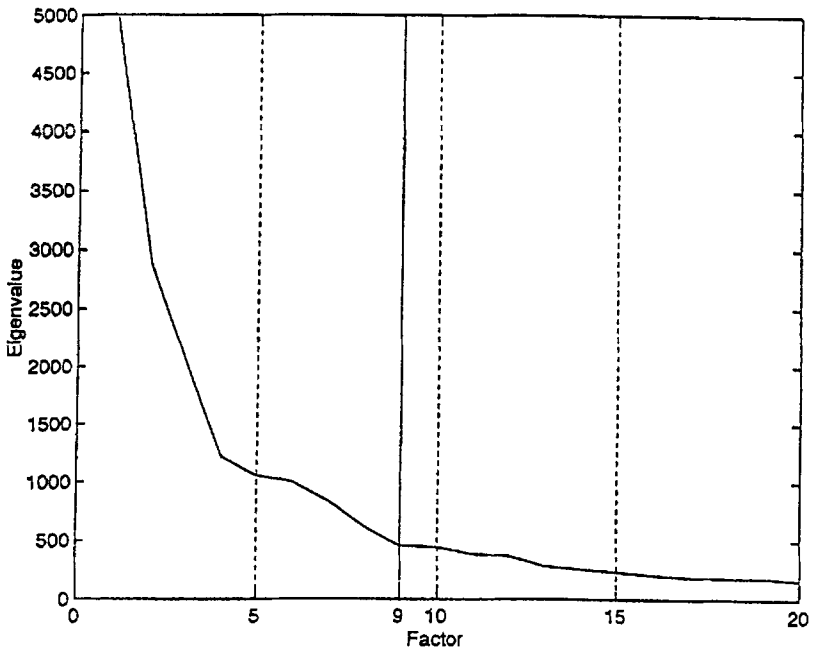

Figure 1. Scree test eigenvalue plot for Case 2a. The slope changes significantly at three places: factor 4, factor 6 and factor 9. Since overfactoring does not significantly affect the rotations, the first nine factors were chosen to be rotated.

profiles, effectively reducing the matrix size by half. This vertical decimation of the profiles is done on each of the four cases mentioned above. For the base case (case 2a), a matrix with every even level is also created. This matrix contains all the levels left out of the main data matrix. Comparison of the PCA results from these two versions of case 2a are used to determine if the results are significantly affected by the choice of which levels to retain. After this step, the rotated PCs are obtained via the Promax method, as described above.

The rotated PCs are multivariate profiles of horizontal velocity perturbations, vertical velocity perturbations, and temperature perturbations. This information will be interpreted directly and used to produce flux profiles and other diagnostic information including two-dimensional (x, y) maps of the PC scores that describe the spectal variation of the contribution of each rotated PC to the original data. The PC scores are just the linear regression coefficients that recombine the PC profiles to reproduce the original data matrix. Thus, there is a PC score associated with each PC (i.e. its coefficient in the linear combination of PCs that reproduce the original data). Because the original data profiles vary with x and y positions in the model domain, the scores for each PC do as well. This variation allows the data profile at each (x, y) gridpoint to be reproduced as a linear combination of the PCs. One can think of this process conversely as well, with each data profile being decomposed into a linear combination of PCs. Because of this x and y variation, each PC's score

is a horizontal map as mentioned above. Both the multivariate vertical structure of the PCs and the horizontal distribution of their importance (as quantified in the corresponding score maps) will be used in our physical interpretation in Section 3 below.

To determine the behaviour of PCA results under adverse conditions, testing was undertaken using a number of artificial data sets created by the authors. PCA was tested for several different potential modes of failure in order to determine the ability of PCA to discern various types of structures in the presence of data behaviour known to be detrimental to its success. In each case, multiple sinusoidal non-orthogonal data profiles were combined using spatially varying random coefficients to create an input data matrix. The impact of signal-to-noise ratio was tested by adding random noise to the data matrix. PCA was able to resolve the original profiles with a signal-to-noise ratio of 0.5 indicating little sensitivity of the results to contamination of the data by unrelated phenomena. PCA does, however, exhibit some shortcomings. PCA frequently requires multiple PCs to describe a single phenomenon, a fact that is seen throughout the LES results. This result occurs whenever a phenomenon's vertical structure varies with horizontal position in each occurrence of the phenomenon (e.g., each thermal updraft is flanked by low level inflow and upper level outflow that, while part of the same phenomenon, have a substantially different multivariate vertical structure than the updrafts themselves). This intrinsic result of the complexity of real three-dimensional phenomena is not in itself a problem. It merely requires that all the PCs associated with a single phenomenon be interpreted together. This characteristic of PCA is magnified, however, when a strong temporal evolution or a strong vertical propagation is present. In the extreme case, the number of PCs that must be retained would approach the number of data points in an input profile (i.e. virtually all PCs would be required to describe the data). As a result, physical interpretation can become unfeasible in the extreme cases as PCA fails to reduce the dimensionality of the data. Tests were conducted to determine the limits beyond which such interpretation is unwise.

There are some guidelines that one should remember when using PCA and interpreting the results. By themselves, the signs of the individual PCs and their corresponding score maps are mathematically arbitrary. This fact results because multiplying both an entire PC and its entire corresponding score map by -1 has no effect on the reconstruction of the data via multiplication of two. Because a PC's scores can be positive in some regions of the map and negative in others, a positive sign for a given variable in the PC is not equivalent to that variable being always positive in the phenomena described by the PC. Thus, the PCs must be multiplied by their corresponding scores before their absolute sign has physical meaning. The vertical profile of relative sign within each PC (and thus the sign changes within each PC) are, however, non-arbitrary and can, therefore, be physically interpreted. For example, a PC that has a negative w perturbation in the lower boundary layer and a positive w perturbation in the upper boundary layer does not always represent a

downdraft underlying an updraft. Because the physical sign of the maxima depends on the sign of the spatially varying score, the PC may represent either an updraft over a downdraft (in the case of a positive score) or a downdraft over an updraft (in the case of a negative score).

Physical interpretation can also be aided by multiplying together the profiles of two variables within a PC to obtain a covariance or flux profile for the PC. This multiplication eliminates the sign ambiguity because the square of -1 is the same as that of 1. Note, however, that this beneficial result occurs only when one multiplies an even number of variables together. For example, the sign of the product of three variables (say w^3) reflects the arbitrary sign of the original PC and can, therefore, be interpreted only in terms of the spatially varying sign of the corresponding score.

3. Results

Physical interpretation of the principal components is based on the resulting variable profiles, the corresponding flux profiles, and the score maps. The first results discussed are from sensitivity tests undertaken to demonstrate the robustness of the method described in the procedures sections. Physical interpretation of the primary results and discussion of their implications for convective boundary-layer turbulence dynamics follows.

The vertical decimation of the original data matrix has no appreciable impact on the results as virtually identical rotated PCs result whether the odd or even numbered levels are retained for analysis. As can be seen in Figure 2, factor 1 in the even-level profile of case 2a (second row of Figure 2) is very similar to factor 1 of the odd-level profile of case 2a (first row of Figure 2). The differences appear to be nothing more than weak, small-scale noise. Moreover, the other PC profiles (not shown) are also highly similar between these two analyses. This similarity is to be expected given the strong dynamic coupling and numerical dependence between adjacent levels in the LES code. This analysis leads to the conclusion that the use of only the odd levels does not hamper the ability to obtain structural information from these LES results.

Structural information is also not lost as a consequence of looking at only one snapshot in time. This result is seen from comparison of two temporally independent cases; case 2a occurs one large-eddy turnover time before case 2b. The third row of profiles in Figure 2 shows the corresponding convective PC from case 2b. Again, the structure is similar. There is a noticeable difference in the amplitude, but not the shape, of the w perturbation maxima of the factors. This suggests that one LES snapshot does not always provide a completely adequate sample size of thermals in all stages of their evolution. However for all other variables the profiles were virtually identical, with the only differences being on a small vertical scale and of a magnitude much less than that of the physical signal for the corresponding variable. This close similarity in profile shape for all variables is an indication that

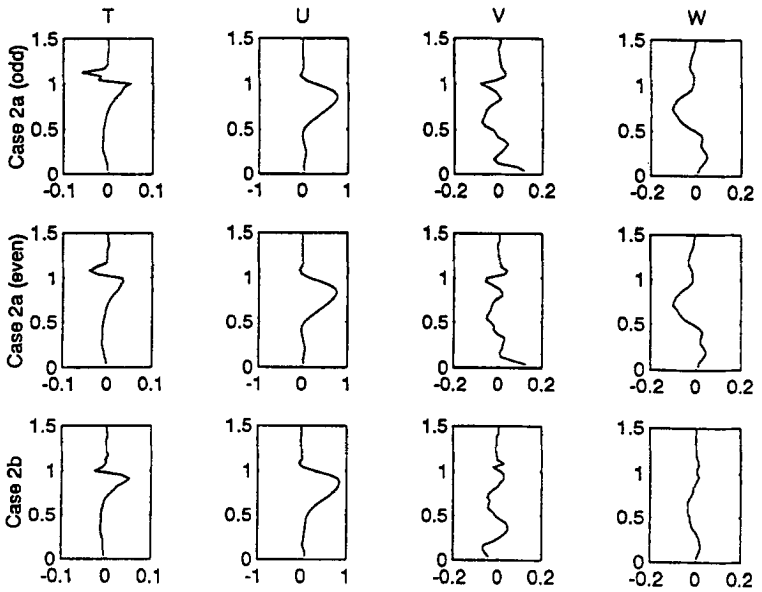

Figure 2. Comparison of the same convective PC for three different cases as a demonstration of the robustness of the method. The first row is factor 1 from case 2a (odd levels). The second row is factor 1 from case 2a (even levels). The third row is the corresponding convective PC, factor 3, from case 2b.

the same phenomena appear at both times and that the LES domain is in fact large enough to provide an adequate sample at both times for qualitative interpretation. Quantitative interpretation of vertical velocity and fluxes requires a larger data set. This finding does not, however, rule out the existence of relatively rare, temporally intermittent, phenomena that have been missed by one or both snapshots.

The PC profiles and the corresponding flux profiles for the moderately convective base case (case 2a) are presented in Figures 3 and 4. In all, there are seven different factors that are found in both snapshots. These factors from case 2a, and their respective matches from case 2b, are listed in Table II. The two factors that do not repeat fall into the relatively rare, temporally intermittent, category mentioned above and should not be discussed based on snapshot analysis. Only the computationally unfeasible analysis of many temporally independent snapshots would provide robust results for this category of phenomenon.

In both case 2a and case 2b, there are five convective PCs and two dynamic PCs. The pairing of corresponding PCs between cases 2a and 2b was determined by examination of the multivariate PC profiles. The members of each pair of corresponding PCs exhibit strong similarities in the elevation and amplitude of the dominant extrema in all variables. The distinction between convective and dynamic PCs is based on the relative contribution of buoyant production/destruction of turbulence kinetic energy (TKE) as seen in the buoyancy flux profiles of Figure 4. These flux profiles are obtained via level-by- level multiplication of the appropriate

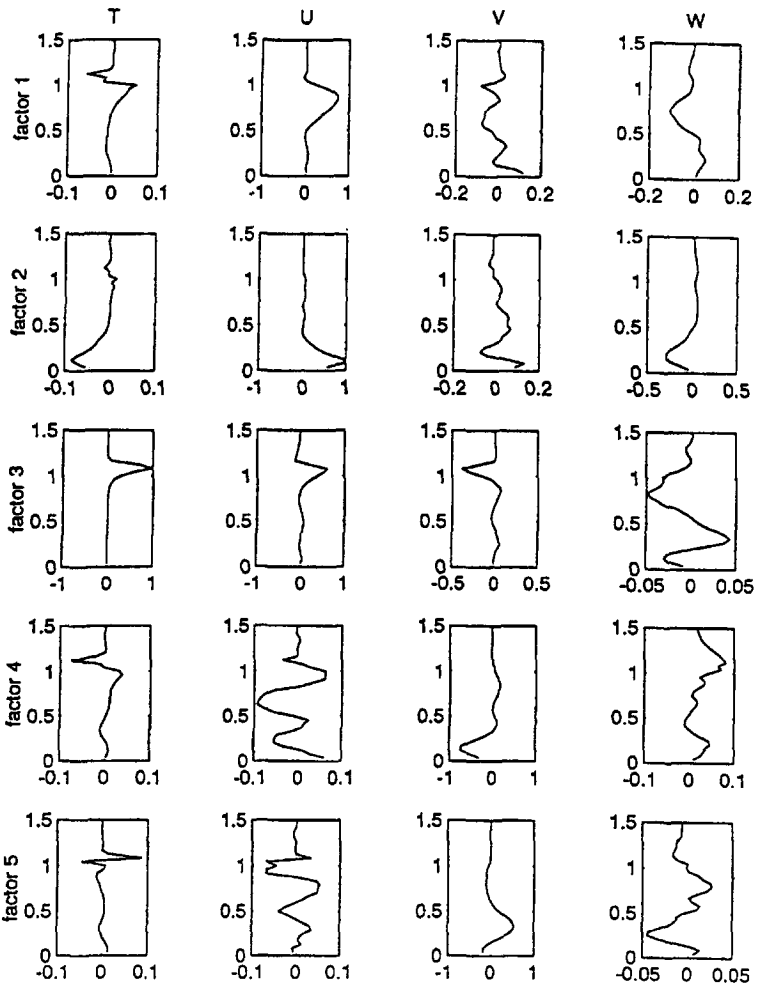

Figure 3. Variable profiles for case 2a. Horizontal axis is the value of perturbations (K for temperature, m s^{-1} for u, v, and w). Vertical axis is height normalized by boundary-layer depth, Z_i. Note the differences in horizontal scale from factor to factor.

two perturbation variables from the multivariate PCs presented in Figure 3. Table II lists the PCs and the type of convective or dynamic process associated with each PC. The corresponding PCs for Case 2a and Case 2b often have different factor (PC) numbers. This temporal change in the PC order can be interpreted as a temporal change in the relative contribution of various eddy types to the turbulence field. For the reasons discussed above, the two temporally intermittent factors are left out of Table II and all subsequent discussion, but it is worth noting that they are thermally neutral dynamic modes.

The thermal structure of the 5 convective PCs (i.e., those PCs that contribute significantly to the convective heat flux at some level) in Figure 3 and Figure 4 are similar to that found in conditional sampling studies of thermals (Young,

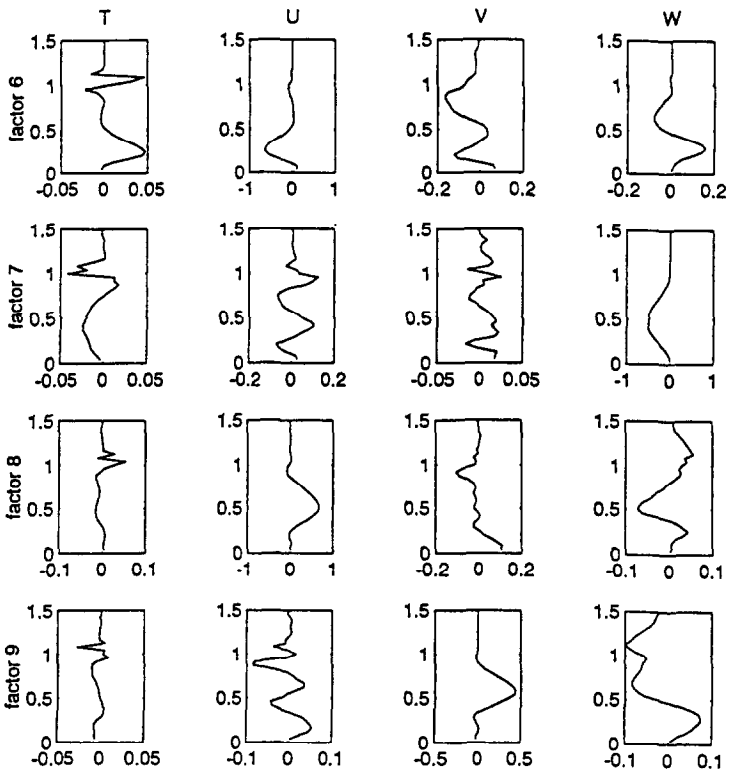

Figure 3. Continued.

Table II

Boundary-layer (BL) phenomena and the corresponding factors from case 2a and case 2b.

Phenomena	Factor number from Case 2a	Factor number from Case 2b
Lower BL convection	2	1
Mid-Low BL convection	6	7
BL spanning convection	7	5
Upper BL convection	1	3
Overshooting convection	3	4
BL mixing (U wind)	8	8
BL mixing (V wind)	5	6

1988; Greenhut and Khalsa, 1987; Schmidt and Schumann, 1990; Schumann and Moeng, 1991a). The dominant extremum of each PC has similar convective flux characteristics (buoyancy flux sign in particular) to previous results for those levels. Each PC describes the aspects of convection as seen in a contiguous range of levels

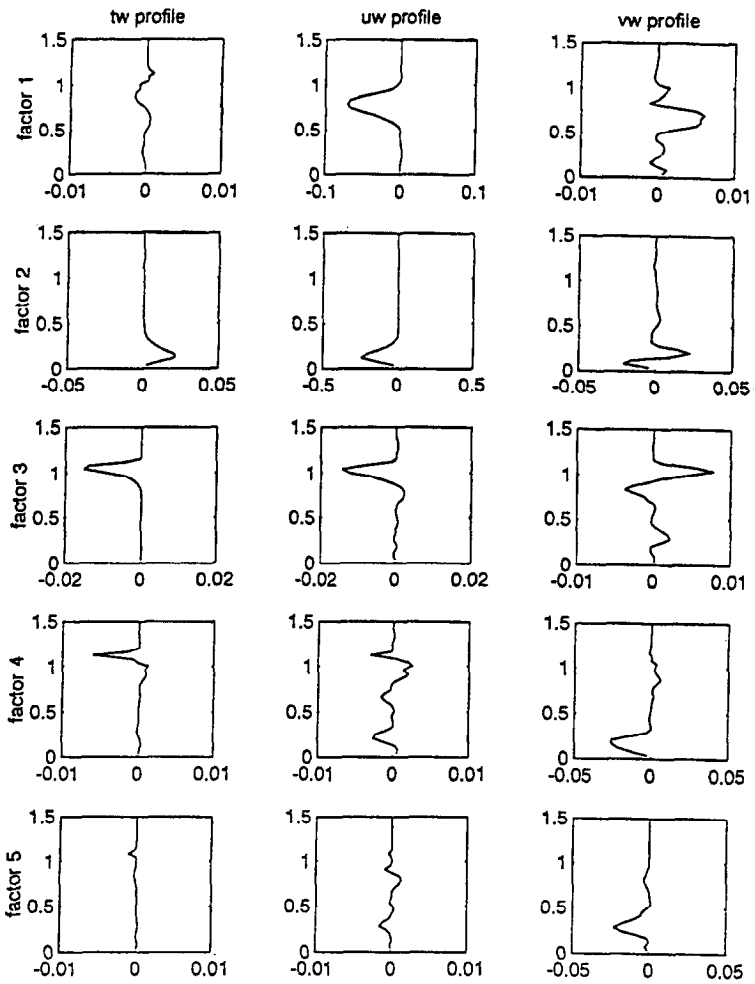

Figure 4. Flux profiles of each factor for case 2a. Horizontal axis is the flux value (K ms^{-1} for temperature flux and m^2s^{-2} for u-momentum and v-momentum flux). Vertical axis is height normalized boundary-layer depth, Z_i. Note the differences in horizontal scale from factor to factor.

around that maxima. Thus, buoyancy (temperature profiles from Figure 3) and buoyant production of TKE (temperature flux profiles from Figure 4) are large and positive in the lower CBL, weakly positive in the middle CBL, and negative in the upper CBL capping inversion. These convective modes have a tendency to be aligned in bands along the direction of the geostrophic wind. This banding, and other morphological characteristics discussed below, are obvious in (x, y) contour maps of the scores (Figure 5). This along-wind banding of relatively three-dimensional cells is typical of regimes intermediate between two-dimensional rolls and three-dimensional cells. The values of $w_*/u_* = 1.69$ and $Z_i/L = -4.8$ for

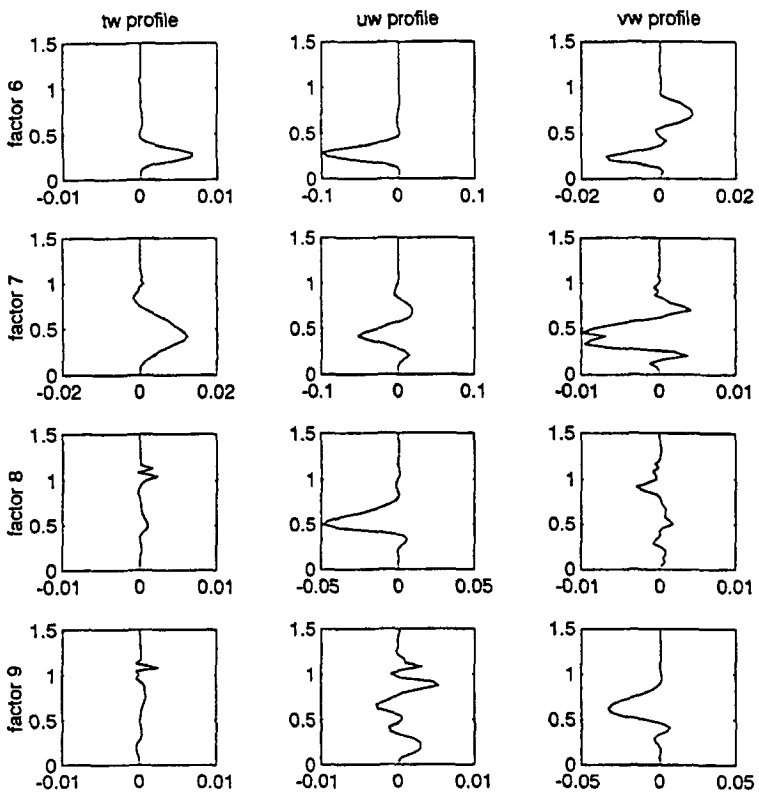

Figure 4. Continued.

case 2a fall near the threshold between these two regimes as discussed by Brown (1980).

The fact that more than one PC is needed to describe the vertical draft structure of a single convective element (i.e. a convective updraft or downdraft) implies that there are significant differences between the multivariate profile of convection at different grid points. These differences could result from variations during the life cycle of the convective elements or from tilting of the convective elements from the vertical. In the former case, a single snapshot would capture various thermals at different phases of their life cycles. In the latter case, the profiles would penetrate the thermals at various levels. Based on analysis of the score maps in Figure 5, it is apparent that while both effects occur, the former possibility dominates for this case. These score maps show numerous three-dimensional convective elements. Each of these elements appears on, at most, two or three score maps for vertically adjacent PCs rather than incorporating all five convective modes. Vertically adjacent PCs are PCs that are adjacent in an ordered set constructed by the elevation of bouyancy flux extrema. Moreover, these multi-PC convective elements have only small random tilts from the vertical as was verified by analyzing the raw LES,

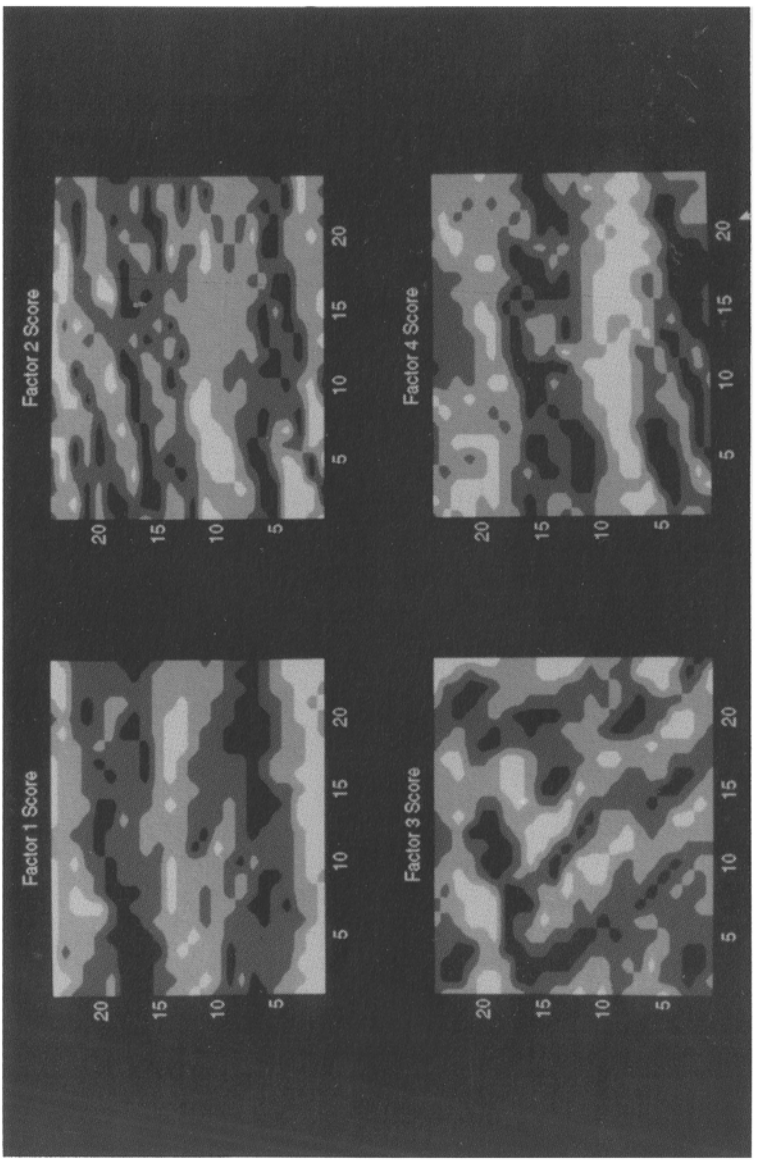

Figure 5. Score maps of the factors for Case 2a. Each score map shows quantitatively how the contribution of one rotated PC varies across the LES domain. Horizontal and vertical axes correspond to the x and y axes of the LES domain. The geostrophic wind is in the x direction. White shading indicates score values greater than 1.0, black shading indicates score values less than -1.0, and grey shading indicates score values between these two thresholds.

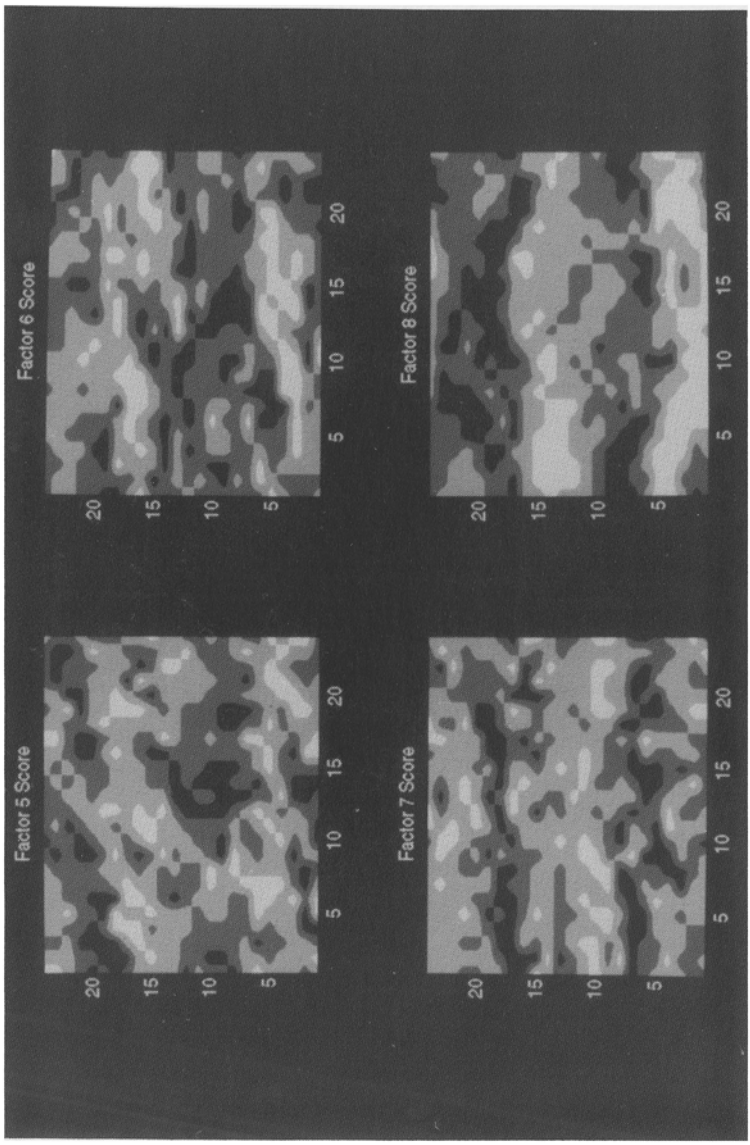

Figure 5. Continued.

and by reconstruction of the data using the retained, rotated PCs. Recall from the discussion in section 2 above that increasing the tilt from the vertical would increase the number of PCs needed to describe a phenomenon. Thus, the score maps in Figure 5 lead to the conclusion that, for this moderately convective regime, PCA is capturing the life cycle of three-dimensional convective elements and their distribution in two-dimensional bands.

Discussion of the individual convective elements will start in the lower boundary and progress upward through the boundary layer and capping inversion. The following discussions, unless otherwise noted, refer to case 2a. In the lowest convective PC (factor 2), most of the convective activity as measured by temperature and vertical velocity perturbations is confined to the lower half of the boundary layer. As expected for lower boundary-layer convective elements (Young, 1988), this factor is thermally direct, as there is a strong positive correlation between perturbations of temperature and vertical velocity in the lowest levels of the boundary layer. This factor also shows a downward flux of u momentum at the same levels, a characteristic phenomenon for the strongly sheared surface layer given a geostrophic wind in the positive x-direction. In this PC, the upper boundary layer is thermally neutral; however, there is a weak counterdraft (remember from Section 2 that the absolute sign of the PCs is arbitrary although the relative sign within the PC has meaning) in the upper boundary layer, as well as a weak counterdraft (a vertically displaced vertical draft of the opposite sign of the main w extremum) present in the layers above the capping inversion. The latter aspect may not be significant as it appears in case 2a only. The multiplication of this PC by its corresponding score map (Figure 5) reveals a number of strong, compact three-dimensional updrafts aligned in two bands that are separated by bands of weaker subsidence with less three-dimensional structure.

The mid-lower boundary-layer convection is described by factor 6 (Figure 3 and Figure 4). This PC is structurally very similar to the lower boundary-layer convective PC. However, the level of the strongest buoyancy flux has been raised by approximately $0.1Z_i$ over that found in factor 2. Also, the strongest buoyancy flux is of slightly lesser magnitude than for factor 2, as expected from the conditional sampling studies cited above. The maximum u-momentum flux is also weaker, and it has risen in the boundary layer to become detached from the surface. This difference can be understood in terms of the decrease of shear (not shown), and therefore shear production of u perturbations with increasing height in the boundary layer. The temperature flux gives an indication of the thermal neutrality of this PC in the upper boundary layer. The score map for factor 6 (Figure 5) begins to show a more organized pattern of three-dimensional updraft cells, aligned more or less in two bands along the geostrophic wind direction. In the other regions of the score map, a general slight subsidence occurs. These bands are shifted slightly northward relative to those of the previous factor, indicating a small tilt in the direction of the shear of the ageostrophic v-component of the wind.

The boundary-layer spanning convective elements are captured by factor 7. This is once again a thermally direct phenomenon. The vertical velocity perturbation extends from the surface to roughly $0.8Z_i$. The vertical velocity above this height is rather small. Below this level, the correlation between temperature and vertical velocity perturbations is still present, but the magnitude has decreased from that seen for factor 2. One prominent feature is the replacement of upper boundary layer neutrality with thermally indirect forcing as the vertical updrafts begin to interact with the inversion-induced stability at those levels. The u-momentum flux has weakened and become erratic. This feature is consistent with mature drafts occurring within a layer of decreased shear. The score map of factor 7 (Figure 5) shows two organized bands of relatively strong updrafts with significant three-dimensional cellular structure superimposed. Once again, in the other regions of the score map, there is general subsidence. These bands are collocated with those for the previous factor.

Factor 1 captures upper boundary-layer convection with the main vertical draft confined to the levels above $0.7Z_i$ (Figure 3). Because the vertical draft lies above the level of neutral buoyancy, the buoyancy flux completes the sign reversal begun in factor 7. Also of interest is the pronounced u-jet, present in the upper half of the boundary layer, that is indicative of renewed shear production as the convection contacts the shear layer across the capping inversion. The complexity of the temperature flux profile is indicative of the overlap of the vertical circulation with the level of neutral buoyancy. The weak u-momentum flux is downward and confined to the upper half of the boundary layer. In contrast, the v-momentum flux is weaker and upward, but these fluxes are confined to the upper half of the boundary layer as well. The sign difference between these two momentum fluxes results from Z_i being significantly less than the potential depth of the ageostrophic flow. When Z_i is less than this depth, the uppermost part of the boundary layer will contain a negative u-shear and positive v-shear (recall that x is aligned with the geostrophic wind), leading to opposite signs for the shear production of these two components of the momentum flux. The score map for factor 1 has a strong two-band signature with moderate three-dimensional cells superimposed. This map indicates bands of general subsidence between the bands of rising air. Thus, the features described by factor 1 are highly consistent with those that are present when convection begins to interact with the sheared inversion that results when the CBL grows to a depth less than that which the ageostrophic flow would have filled had Z_i not intervened.

The final convective PC, factor 3 (Figures 3 and 4), represents overshooting convection and entrainment events. This factor describes the processes that occur when thermals overshoot their level of neutral buoyancy, thereby perturbing the capping inversion. The profiles of temperature, u and v all have a significant perturbation at or just above Z_i. Elsewhere in the boundary layer, perturbations of these variables are near zero. Vertical velocities for factor 3 are weak, suggesting they represent parcels near the end of their vertical excursions above or below their buoyant equilibrium level. These weak vertical motions are, however, ther-

mally indirect, indicating that entrainment into the overshooting parcels causes a detectable decrease in the magnitude of the parcel buoyancy. As with the upper boundary-layer convection (factor 1), shear production results in a downward flux of u momentum and an upward flux of v momentum. In sharp contrast to the banding present in the other convective PCs, the score map shows three-dimensional cells of updrafts and downdrafts distributed in no particular pattern. This unexpected result is conjectured to be a consequence of cross-roll advection of parcels during the long residence time near the inversion as they move from the roll updrafts' locations to those of the roll downdrafts. Another possible mechanism for this result is constructive interference patterns between gravity waves radiating from the disturbances in the inversion caused by impinging three-dimensional updraft cells.

Taken together, these PCs and their score maps quantify the overall morphology of the convection for this regime as three-dimensional cells embedded in two-dimensional rolls. These rolls are aligned parallel to the geostrophic wind and have little or no tilt with height due to shear in the ageostrophic wind except in the lowest levels where the rolls tilt downshear. The three-dimensional cells also exhibited little systematic tilt from the vertical. In the LES results, it was rare to see a thermal extend all the way from the surface layer to the capping inversion, suggesting that PCA captures the life cycle of bubble-like convective elements. The details of the convective element morphology have a profound impact on gravity wave generation as discussed next.

Gravity wave signatures appear on various factors in this analysis. The v perturbation profile from factor 1 has a peak at the top of the entrainment zone (i.e., the top of the capping inversion) which decays exponentially above that level. The w-perturbation profile from factor 4 also has a similar peak at the top of the entrainment zone that decays exponentially above the inversion. The occurrence of these gravity wave components on different PCs suggest that they are out of phase in the horizontal, which is consistent with gravity wave theory (Holton, 1979). The existence of a v-perturbation above the entrainment zone with sign opposite to that in the underlying convective boundary layer creates enhanced shear across the inversion, as seen in Rayment and Readings (1974). The score map (Figure 5) shows the w-component of the gravity waves to be oriented in banded couplets centered on the banded convective updrafts, with the updraft on the north (upshear) side. This pattern can be understood by assuming that the rolls are drifting with the boundary-layer flow, including the northward (cross-roll) component of the Ekman drift, effectively creating a moving mountain ridge in the free atmosphere. This phenomenon has been labeled a convection wave (Clark *et al.*, 1986; Noilhan *et al.*, 1986; Kuettner *et al.*, 1987; Balaji and Clark, 1988; Redelsperger and Clark, 1990). Given this relative phasing between the w-component of the gravity wave and the convective components, it is only to be expected that some of the v component of the inflow and outflow of the two-dimensional rolls would be captured by the same factor (factor 4), which indeed it is.

There are two dynamic PCs, specifically PCs that do not feature a significantly thermally direct and/or thermally indirect circulation at any level. Factor 8 (a mid-boundary layer u-jet) and factor 5 (a mid-boundary layer v-jet) have near-neutral buoyancy, and consequently buoyancy fluxes an order of magnitude weaker than those of the convective PCs at all levels. The u-jet (factor 8) extends from about 0.2 to $0.8Z_i$, and has a downward flux of u momentum. The fluxes of temperature and of v momentum are weak and erratic. At levels below $0.3Z_i$ this factor has a significant v-component, which is shown below to describe some of the inflow into the two-dimensional convective updrafts. There is a v-component of opposite sign between 0.8 and $1.0Z_i$ that is shown to describe some of the outflow from these updrafts. The score map for this factor shows a dipole banded structure centered on the convective updraft bands. These bands are distributed so that their centres lie closer to the updrafts than to the downdrafts. The signs of the positive and negative bands are such that lower boundary-layer v flow is directed from the downdrafts to the updrafts as expected from continuity considerations. The inflow couplet is concentrated near the updraft. Thus, this component represents the inflow into the two-dimensional updrafts, which must be out of phase horizontally, and hence on a different PC, from the convective updrafts. This phasing also results in middle boundary-layer cyclonic shear vorticity ($\partial u/\partial y < 0$) across the updraft bands. Thus, while not contributing significantly to the buoyancy flux or buoyant production of TKE, this "dynamic" PC is an integral part of the convective circulation of the longitudinal rolls. The distinction between "dynamic" and "convective" in this case follows from the PC's role in the eddy rather than the fundamental dynamics of the eddy type to which it contributes.

The v-jet has a similar structure. The v-jet (factor 5) is, however, slightly weaker in magnitude and occurs somewhat lower in the boundary layer. The v-momentum flux is downward and smaller in magnitude than is the u-momentum flux of the u-jet. The temperature flux and the flux of the u momentum are weak and erratic for the v-jet. The score map is dominated by three-dimensional cells that appear to be unrelated to the two-dimensional rolls.

A second case, case 5, in approximately the same dynamic regime as case 2a is examined to determine if the results discussed above are sensitive to small changes in the scaling parameters which describe the forcing. The results from case 5 are very similar to those of case 2a despite the slightly weakened convective forcing reflected in the w_* values of Table I. Despite the weakened convection, the five convective and two dynamic modes were still produced.

The convective PCs from case 5 (not shown) produce temperature and vertical velocity patterns that are structurally similar to those in case 2a. However, the magnitude of the perturbations are weakened, particularly in the upper and lower boundary layer. Consequently, the lower to middle boundary-layer fluxes are significantly reduced. The temperature fluxes in the upper boundary layer are more closely linked to inversion characteristics than to surface fluxes (Stull, 1976). Summarizing, a decrease in convective forcing (from a temperature flux of 0.05

Table III
Boundary-layer (BL) phenomena and the corresponding factors from case 4.

Phenomena	Factor number from Case 4
Lower BL convection	1
BL spanning convection	6
Overshooting convection	8
BL mixing (U wind)	5
BL mixing (V wind)	9

to 0.03 K ms^{-1}, and w_* from 0.94 to 0.78 ms^{-1} did not qualitatively change the convection, and the quantitative changes were minor.

The dynamic PCs from case 5 are only slightly modified, as expected from the minimal changes in u_* and w_* values. The PC that describes the u-jet is similar to that from case 2a. However, its peak is slightly higher in the boundary layer and it has an increased magnitude. The v-jet exhibits a similar shift in elevation and similar change in magnitude. In both these PCs, neutral buoyancy is observed throughout the boundary layer. Thus, the minor dynamic and convective forcing changes between case 2a and case 5 are not significant enough to produce qualitative changes in the dynamic PCs, and the quantitative changes were minor.

Figure 6 and Figure 7 show the PCs and the corresponding flux profiles, respectively, for the highly convective case 4. In case 4, the convective forcing is increased drastically to 0.24 K ms^{-1}, more than doubling w_*, while u_* remained nearly unchanged (Table I). This change produced significant changes in the convection. Only three convective PCs (Table III) are needed, rather than the five required for the other cases. The lower to middle, and upper, boundary-layer convection PCs are no longer needed to describe the convective modes, the increased forcing having simplified the vertical structure of the convective elements. The bubble-like convective elements have become deeper (relative to the boundary-layer depth) and stronger. This deepening of the convective elements could be resolved using conventional conditional sampling or compositing approaches only if they used simultaneous vertically stacked observations as was done by Schumann and Moeng (1991a, b) using LES results. Their sampling criteria did not, however, take into account variable thermal age or variable tilt from the vertical, and thus resulted in a blending together of the different components which PCA is able to distinguish. This shortcoming is not insoluble, as more advanced sampling criteria could be developed for the generation of results comparable to those of PCA.

The increase in the convective forcing causes a significant, but expected, change in the lower boundary-layer convective PC. Factor 1 shows an increase in the buoyancy magnitude of these convective elements, with a resultant increase in vertical

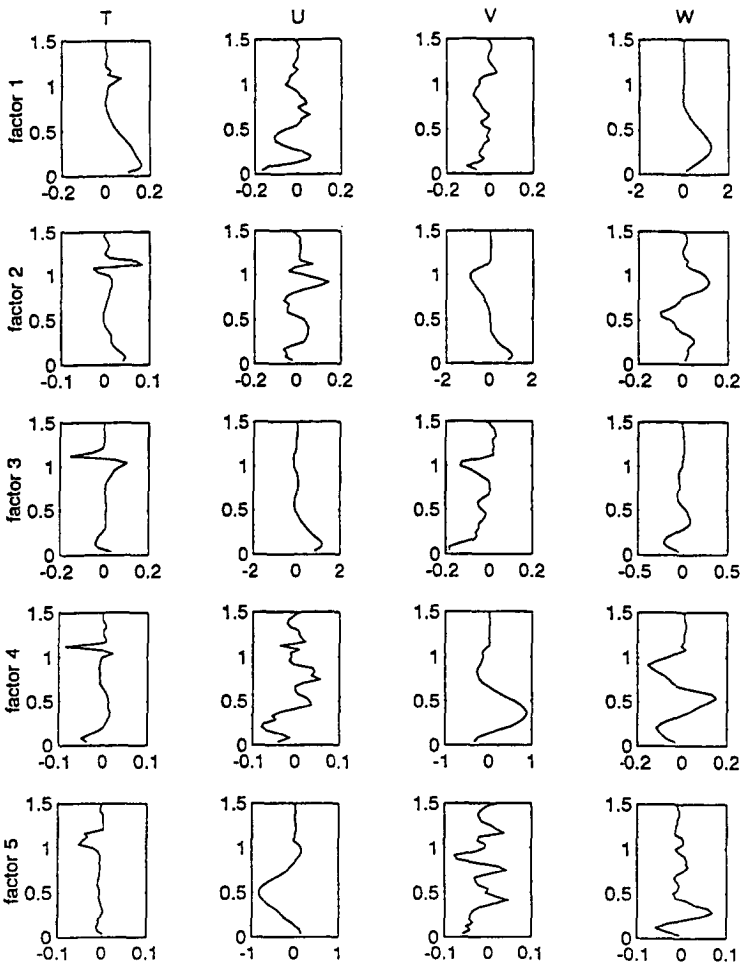

Figure 6. Variable profiles from case 4. Axes as in Figure 1.

velocity perturbations. The depth of this convective component has also increased, as is required if only three PCs are needed to span the boundary-layer depth. As a result of these changes, the temperature flux profile possesses a stronger, more elevated peak. The flux of u momentum by the lower boundary-layer convective PC is weaker than in case 2a because the vertical velocity peak is farther elevated away from the surface layer.

The boundary layer spanning convective PC (factor 6) has undergone similar transformations (Figured 6 and 7). The peaks in buoyancy and in vertical velocity are much stronger and significantly higher than in the corresponding factor (factor 7) in case 2a (Figure 3). Both are detached from the surface. The u-perturbation profile looks similar to that in case 2a; however, the profile has shifted upward in the boundary layer in conjunction with a shift in the vertical velocity profile. The v-

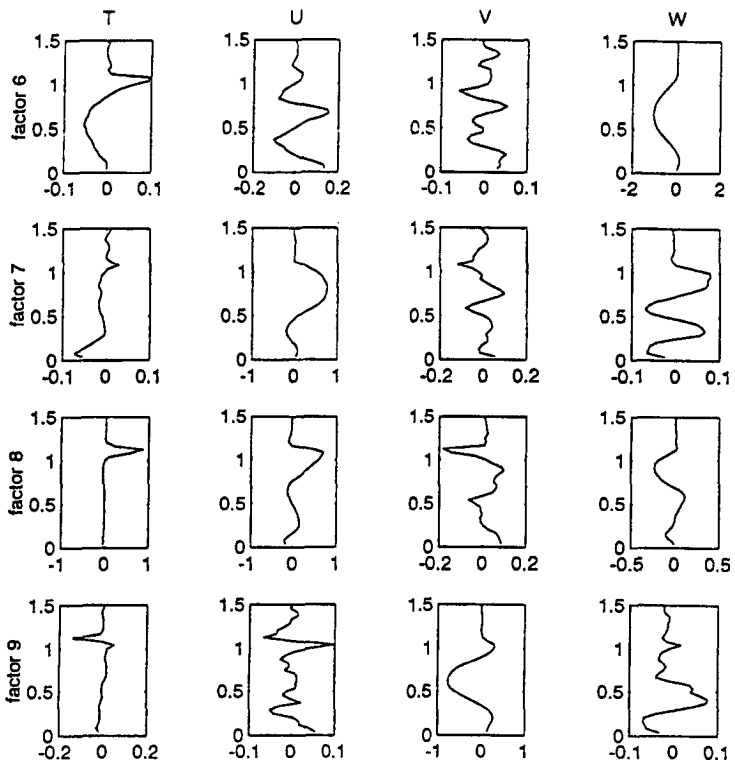

Figure 6. Continued.

perturbation wind profile, which is weak and erratic, bears little resemblance to the profile in case 2a. Thus, the increase in buoyancy forcing causes a general lifting and intensification of the PC that describes boundary-layer spanning convective elements.

The overshooting convection PC, factor 8, produces inversion level peaks not unlike those in case 2a (factor 3). The peaks for u perturbation and temperature perturbation at the inversion have similar amplitudes, but the v perturbation at the inversion peak is stronger than in case 2a. The boundary-layer updraft–downdraft couplet is present in this profile, and it is stronger than in case 2a. As in case 2a, there is a spike of u-momentum flux and v-momentum flux at the inversion.

Factor 2 captures the north-south component of convective inflow and outflow. It is comparable to the corresponding component for case 2a (factor 4), except that there is no hint of gravity-wave perturbations above the boundary layer. The score map (Figure 8) of factor 2, and case 4 in general, exhibits no roll-like structure. Rather, the three-dimensional convective cells are randomly distributed and not organized into two-dimensional rolls as in case 2a.

The dynamic PCs did not undergo the dramatic transformations that the convective PCs did. The u-jet has similar structures as that of case 2a, including counter

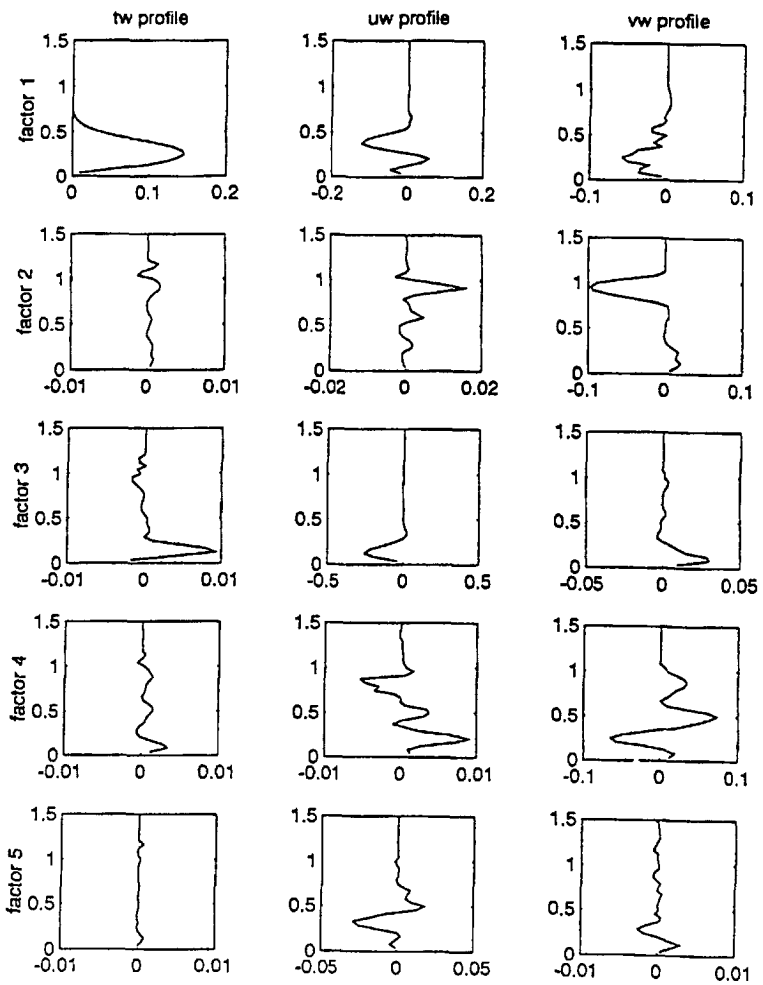

Figure 7. Flux profiles from case 4. Axes as in Figure 2.

jets near the surface and the inversion. The u-jet (factor 5) is a bit stronger and slightly closer to the surface. The u-momentum flux profile is similar but it has a higher peak. The other fluxes remain insignificant. The v-jet (factor 9) is virtually identical to the v-jet found in case 2a. Thus, these dynamic modes do not appear to be sensitive to the morphology and alignment of the convective elements.

Comparison of case 4 with case 2a and case 5 leads to fundamental insights into boundary-layer processes. To summarize, the sharp increase in w_* (and therefore w_*/u_*) simplified the vertical structure of the three-dimensional convective elements, while the horizontal structure became more complex. The increased convective forcing also changed the entrainment fluxes of u and v momentum at the inversion, but had little or no effect on the dynamic modes involving primarily u and v. From these intercomparisons, it can be deduced that, for this range of

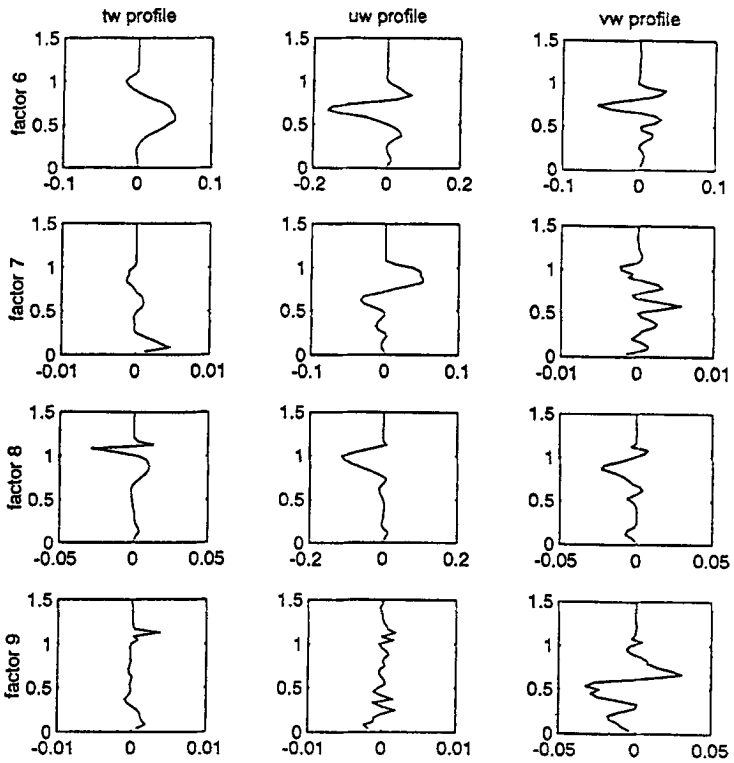

Figure 7. Continued.

forcings, shear affects the form of the convection more than buoyancy affects the form of the dynamic modes.

4. Conclusions

Large eddy simulation (LES) data were analyzed using obliquely rotated principal component analysis (PCA) to find coherent structures in the convective boundary layer. Three different runs of the LES data were used: a moderately convective case (temperature flux about 0.05 K ms^{-1}); a less convective case (0.03 K ms^{-1}); and a highly convective case (0.24 K ms^{-1}). Single snapshots were analyzed for the later two runs, based on the sensitivity/robustness tests made on two snapshots (separated by one eddy turnover time) from the moderately convective case.

Similar convective and dynamic modes were captured in different LES data sets. The moderately convective base case required five convective modes to describe the life cycle of a boundary-layer convective updraft/downdraft element and two dynamic modes to describe the thermally neutral aspects of the boundary-layer turbulence structure. These modes were robust in that they were present for both

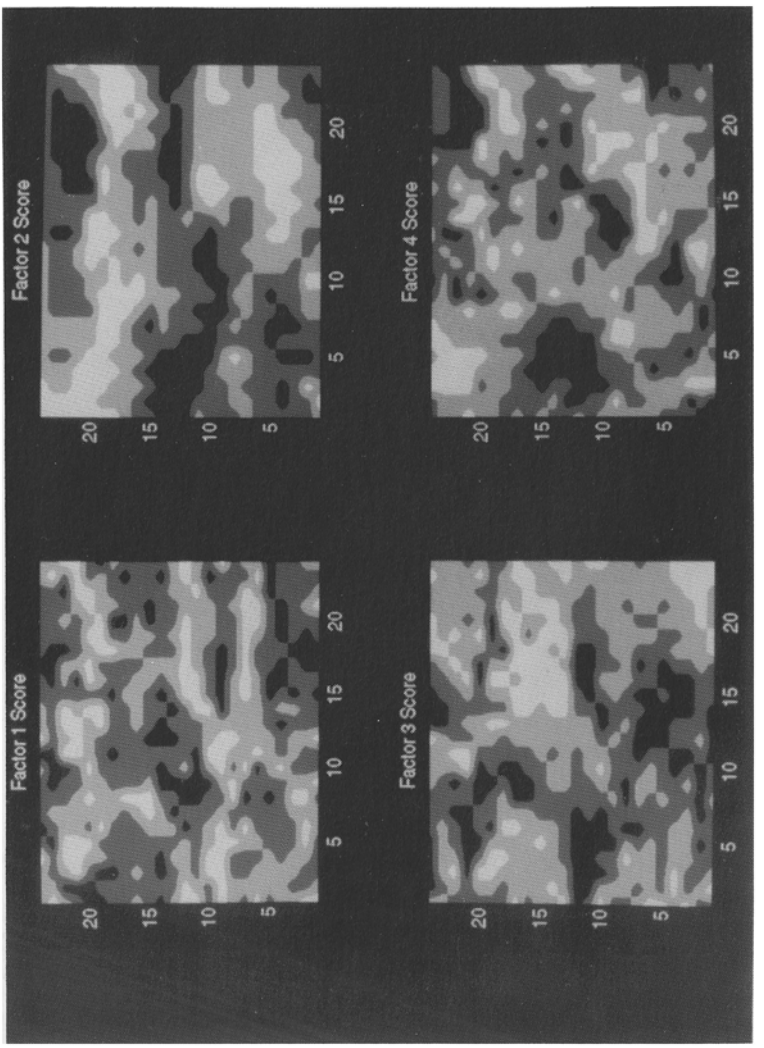

Figure 8. Score maps of each factor for Case 4. Axes and shading as in Figure 4.

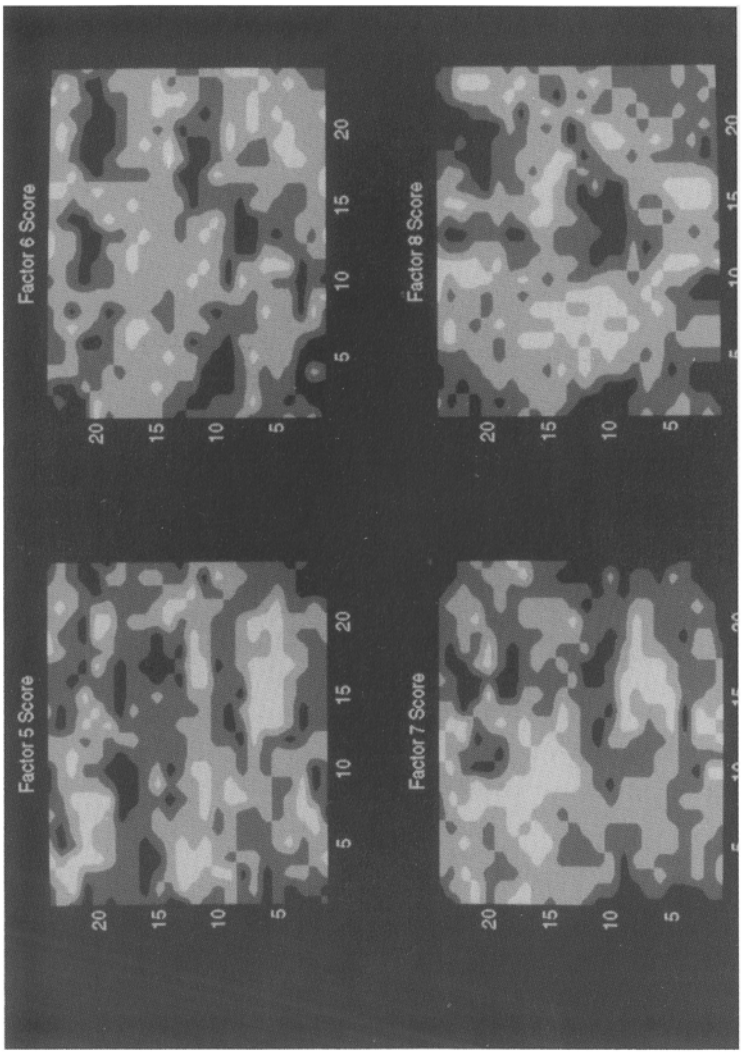

Figure 8. Continued.

temporally independent snapshots of the base case as well as in the slightly less convective run. In contrast, the highly convective LES run required only three convective modes but produced the same two dynamics modes as the previous cases. Score maps demonstrated that the three-dimensional convective cells in the base case were aligned into two-dimensional rolls. Although it is not clear from the PC profiles alone whether the multiple convective PCs reflect the eddy life cycle or a significant tilt from the vertical of the updraft–downdraft axes, examination of the corresponding score maps indicates that both aspects contribute, with the former dominating.

While the inter-run change in w_*/u_* (and hence the change in convective forcing) produced noticeable changes in the form of the convection, the dynamic modes did not undergo radical changes. The dynamic modes, while remaining structurally similar, increased in magnitude slightly with the decrease in convective forcing. An increase in the relative importance of buoyancy to shear (w_*/u_*) simplifies the convective structure in the vertical while the horizontal structure becomes more complex. Thus, at any given point in its life cycle, a convective element has greater depth (relative to Z_i) when buoyancy dominates shear. Therefore, the form of convective updraft/downdraft elements and the PCs that describe them is more sensitive to the ratio of buoyant to shear production than is the form of the dynamic mode.

The LES data were used to test the utility of principal component analysis for convective boundary-layer coherent structure analysis with as complete a data set as possible. These tests demonstrated that the results of the new method agree with results of prior methods such as conditional sampling and composite analysis. PCA, however, provides new insights that are not obtainable with previous analysis methods. In the immediate future, this method will be applied to tower data from field experiments, in particular the RASEX field experiment. While the use of observational data in the follow-on study will avoid LES resolution-induced errors (particularly in the surface layer), it will, of necessity, limit the depth sampled and eliminate the highly useful two-dimensional score maps that are obtainable only from a three-dimensional data set. As so often in convective boundary-layer studies, a careful intercomparison of LES and observational results will permit a synergistic use of the best facets of both data sources.

Acknowledgments

The authors would like to thank Dr. D. Keith Wilson for supplying analysis programs and general help. We would like to thank Dr. John C. Wyngaard for the use of the LES data. We would also like to thank Dr. Hampton N. Shirer and Nathaniel S. Winstead for their collaborations. The ideas of Jim Wilczak and an anonymous reviewer also contributed to this work. This work is supported by the Office of Naval Research through grants N00014-93-1-0252 and N00014-93-1-1123.

References

Balaji, V. and Clark, T. L: 1988, 'Scale Selection in Locally Forced Convective Fields and the Initiation of Deep Cumulus', *J. Atmos. Sci.* **45**, 3188–3211.

Brown, R. A.: 1980, 'Longitudinal Instabilities and Secondary Flows in the Planetary Boundary Layer: A Review', *Rev. Geophys. Space Phys.* **18**, 683–697.

Burroughs, G. E. R. and Miller, H. W. L.: 1961, 'The Rotation of Principal Components', *Brit. J. Stat. Pyschol.* **14**, 35–49.

Cattell, R. B.: 1958, 'Extracting the Correct Number of Factors in Factor Analysis', *Educ. Psychol. Meas.* **18**, 791–838.

Cattell, R. B. and Dickman, K: 1962, 'A Dynamical Model of Physical Influences Demonstrating the Necessity of Oblique Simple Structure', *Psychol. Bull.* **59**, 389–400.

Clark, T. L., Hauf, T., and Kuettner, J. P.: 1986, 'Convectively Forced Internal Gravity Waves: Results From Two Dimensional Experiments', *Quart. J. Roy. Meteorol. Soc.* **112**, 899–926.

Deardorff, J. W.: 1972, 'Numerical Investigation of Neutral and Unstable Planetary Boundary Layers', *J. Atmos. Sci.* **29**, 91–115.

Deardorff, J. W. and Yoon, S.-C.: 1984, 'On the Use of an Annulus to Study Mixed Layer Entrainment,' *J. Fluid Mech.* **142**, 97–120.

Dingman, H. F., Miller, C. R., and Eyman, R. K, 1964, 'A Comparison between Two Analytical Rotational Solutions where the Number of Factors is Indeterminate', *Behav. Sci.* **9**, 76–80.

Greenhut, G. K. and Khalsa, S. J. S.: 1982, 'Updraft and Downdraft Events in the Atmospheric Boundary Layer over the Equatorial Pacific Ocean', *J. Atmos. Sci.* **39**, 1803–1818.

Greenhut, G. K. and Khalsa, S. J. S.: 1987, 'Convective Elements in the Marine Atmospheric Boundary Layer. Part I: Conditional Sampling Techniques', *J. Climate Appl. Meteorol.* **26**, 813–822.

Holton, J. R.: 1979, *An Introduction to Dynamic Meteorology*, Academic Press, 391 pp.

Jolliffe, I. T.: 1987, 'Rotation of Principal Components: Some Comments', *J. Climatol.* **7**, 507–510.

Kaimal, J. C., Wyngaard, J. C., Haugen, D. A., Cote, O. R., Izumi, Y., Caughey, S. J., and Readings, C. J.: 1976, 'Turbulence Structure in the Convective Boundary Layer', *J. Atmos. Sci.* **33**, 2152–2169.

Khalsa, S. J. S.: 1980, 'Surface Layer Intermittency Investigated with Conditional Sampling', *Boundary-Layer Meteorol.* **19**, 509–532.

Khalsa, S. J. S. and Greenhut, G. K: 1985, 'Conditional Sampling of Updrafts and Downdrafts in the Marine Atmospheric Boundary Layer', *J. Atmos. Sci.* **42**, 2550–2562.

Khalsa, S. J. S. and Greenhut, G. K: 1987, 'Convective Elements in the Marine Atmospheric Boundary Layer. Part II: Entrainment at the Capping Inversion', *J. Climate Appl. Meteorol.* **26**, 824–836.

Kuettner, J. P., Hildebrand, P. A., and Clark, T. L.: 1987, 'Convection Waves: Observations of Gravity Wave Systems over Convectively Active Boundary Layers', *Quart. J. Roy. Meteorol. Soc.* **113**, 445–468.

Lenschow, D. H. and Stephens, P. L.: 1980, 'The Role of Thermals in the Convective Boundary Layer', *Boundary-Layer Meteorol.* **19**, 509–532.

Moeng, C.-H.: 1984, 'A Large Eddy Simulation Model for the Study of Planetary Boundary Layer Turbulence', *J. Atmos. Sci.* **41**, 2052–2062.

Moeng, C.-H., and Schumann, U.: 1991, 'Composite Structure of Plumes in Stratus- topped Boundary Layer', *J. Atmos. Sci.* **48**, 2280–2291.

Noilhan, J., Benech, B., Letrenne, G., Druilhet, A., and Saab, A.: 1986, 'Experimental Study of an Artificial Thermal Plume in the Boundary Layer. Part 2: Some Aspects of the Plume Thermodynamic Structure', *J. Climate Appl. Meteorol.* **25**, 439–457.

Rayment, R. and Readings, C. J.: 1974, 'A Case Study of the Structure and Energetics of an Inversion', *Quart. J. Roy. Meteorol. Soc.* **100**, 221–223.

Redelsperger, J. L. and Clark, T. L.: 1990, 'The Initiation and Horizontal Scale Selection of Convective over Gently Sloping Terrain', *J. Atmos. Sci.* **47**, 516–541.

Richman, M. B.: 1986, 'Rotation of Principal Components', *J. Climatol.* **6**, 293–335.

Schmidt, H. and Schumannl U.: 1989, 'Coherent Structure of the Convective Boundary Layer Derived from the Large Eddy Simulation', *J. Fluid Mech.* **200**, 511–562.

Schumann, U. and Moeng, C.-H.: 1991a, 'Plume Fluxes in the Clear and Cloudy Convective Boundary Layers', *J. Atmos. Sci.* **48**, 1746–1757.

Schumann, U. and Moeng, C.-H.: 1991b, 'Plume Budgets in the Clear and Cloudy Convective Boundary Layers', *J. Atmos. Sci.* **48**, 1758–1770.

Sikora, T. D. and Young, G. S.: 1993, 'Observations of Planview Flux Patterns within Convective Structures of the Marine Atmospheric Surface Layer', *Boundary-Layer Meteorol.* **65**, 273–288.

Stull, R. B.: 1976, 'The Energetics of Entrainment Across a Density Interface', *J. Atmos. Sci.* **33**, 1260–1267

Weijers, E. P., van Delden, A., Vugts, H. F., and Meesters, A. G. C. A.: 1995, 'Characteristics of Convective Turbulence in the Surface Layer Investigated by Principal Component Analysis', *J. Appl. Meteorol.* **34**, 528–541.

Wilczak, J. M.: 1984, 'Large Scale Eddies in the Unstably Stratified Atmospheric Surface Layer. Part I: Velocity and Temperature Structure', *J. Atmos. Sci.* **41**, 3537–3550.

Wilczak, J. M. and Tillman, J. E.: 1980, 'The Three Dimensional Structure of Convection in the Atmospheric Surface Layer', *J. Atmos. Sci.* **37**, 2424–2443.

Young, G. S.: 1988, 'Turbulence Structure of the Convective Boundary Layer. Part II: Phoenix 78 Aircraft Observations of Thermals and Their Environment', *J. Atmos. Sci.* **45**, 727–735.